J Biomol NMR (2014) 59:57–73
DOI 10.1007/s10858-014-9824-4

ARTICLE

Sensitivity gains, linearity, and spectral reproducibility in nonuniformly sampled multidimensional MAS NMR spectra of high dynamic range

Christopher L. Suiter · Sivakumar Paramasivam · Guangjin Hou · Shangjin Sun · David Rice · Jeffrey C. Hoch · David Rovnyak · Tatyana Polenova

Received: 13 November 2013 / Accepted: 20 March 2014 / Published online: 22 April 2014

Abstract Recently, we have demonstrated that considerable inherent sensitivity gains are attained in MAS NMR spectra acquired by nonuniform sampling (NUS) and introduced maximum entropy interpolation (MINT) processing that assures the linearity of transformation between the time and frequency domains. In this report, we examine the utility of the NUS/MINT approach in multidimensional datasets possessing high dynamic range, such as homonuclear ^{13}C–^{13}C correlation spectra. We demonstrate on model compounds and on 1–73-(U-^{13}C,^{15}N)/74–108-(U-^{15}N) *E. coli* thioredoxin reassembly, that with appropriately constructed 50 % NUS schedules inherent sensitivity gains of 1.7–2.1-fold are readily reached in such datasets. We show that both linearity and line width are retained under these experimental conditions throughout the entire dynamic range of the signals. Furthermore, we demonstrate that the reproducibility of the peak intensities is excellent in the NUS/MINT approach when experiments are repeated multiple times and identical experimental and processing conditions are employed. Finally, we discuss the principles for design and implementation of random exponentially biased NUS sampling schedules for homonuclear ^{13}C–^{13}C MAS correlation experiments that yield high-quality artifact-free datasets.

Electronic supplementary material The online version of this article (doi:10.1007/s10858-014-9824-4) contains supplementary material, which is available to authorized users.

C. L. Suiter · S. Paramasivam · G. Hou · S. Sun · T. Polenova (✉)
Department of Chemistry and Biochemistry, University of Delaware, Newark, DE 19716, USA
e-mail: tpolenov@udel.edu

C. L. Suiter
e-mail: csuiter@udel.edu

S. Paramasivam
e-mail: siva@udel.edu

G. Hou
e-mail: hou@udel.edu

S. Sun
e-mail: shangjin@udel.edu

C. L. Suiter · G. Hou · T. Polenova
Pittsburgh Center for HIV Protein Interactions, University of Pittsburgh School of Medicine, Pittsburgh, PA 15261, USA

Present Address:
S. Paramasivam
Department of Astrophysics, Pondicherry University, Puducherry 605 014, India

Present Address:
S. Sun
Structural Biophysics Laboratory, Center for Cancer Research, National Cancer Institute, Frederick, MD, USA

D. Rice
Agilent Technologies Inc., Santa Clara, CA 95051, USA
e-mail: dave.rice@agilent.com

J. C. Hoch
Department of Molecular Biology and Biophysics, University of Connecticut Health Center, Farmington, CT 06030-3305, USA
e-mail: hoch@uchc.edu

D. Rovnyak
Department of Chemistry, Bucknell University, Lewisburg, PA 17837, USA
e-mail: drovnyak@bucknell.edu

Keywords NUS · Nonuniform sampling · Sensitivity · Linearity · Magic angle spinning · Dynamic range

Introduction

Homonuclear ^{13}C–^{13}C correlation experiments are widely employed in solid-state MAS NMR for resonance assignments and derivation of distance restraints in biological solids. These experiments are often used as a "fingerprint" for the system of interest, and help to determine the feasibility of more detailed structural and dynamics studies. In many biological systems of interest to a solid-state NMR spectroscopist (e.g., large proteins, membrane proteins, and protein assemblies), inherently low sensitivity requires signal averaging which may take several days for a single 2D homonuclear dataset. These demands on total experimental time are further exacerbated by the use of a large spectral width in ^{13}C–^{13}C spectra at high static field strengths, requiring short t_1 increment times for conventional uniformly sampled (US) spectra and necessitating collection of several hundred uniform increments in the indirect dimension to cover the spectral width and attain the required resolution.

An alternative approach to the acquisition of conventional US spectra, subsequently processed with the fast Fourier transform (FFT), is recording datasets by nonuniform sampling (NUS) (Hoch et al. 2012). NUS is commonly used in MRI and solution NMR spectroscopy (Atreya and Szyperski 2005; Coggins et al. 2010; Hyberts et al. 2007; Kazimierczuk et al. 2010; Maciejewski et al. 2006; Mansfield 1984; Schmieder et al. 1993), and is currently gaining momentum in solid-state MAS NMR as well (Franks et al. 2010; Jones and Opella 2006; Lin and Opella 2013; Matsuki et al. 2009, 2010; Paramasivam et al. 2012; Rovnyak et al. 2003). One attractive feature of NUS is that the requirement to sample the data points along an equally spaced grid during the indirect acquisition period is removed. The experiment time saved is then equal to the number of removed points multiplied by the time it takes to acquire each indirect-dimension point. As we have shown recently, with random exponentially biased NUS schedules, inherent time-domain sensitivity gains are attained when the experiment time is the same as in the uniformly sampled experiment (Paramasivam et al. 2012; Rovnyak et al. 2011). This inherent sensitivity enhancement can be tuned to some extent by the careful design of the sampling schedules (Rovnyak et al. 2004, 2011). At the same time, the line widths are comparable to those in the US experiments when the points are sampled to πT_2^*, a limit readily attained in many MAS NMR applications.

For processing NUS datasets, FFT is not suitable, and a variety of protocols have been proposed for data sampled on- versus off-grid (Balsgart and Vosegaard 2012; Daniell and Hore 1989; Davies et al. 1988; Dereppe and Jakus 1988; Donoho et al. 1990; Eghbalnia et al. 2005; Hiller et al. 2005; Hoch 1985; Hoch and Stern 1996; Hoch et al. 1990; Holland et al. 2011; Hore 1985; Hyberts et al. 2007, 2009, 2012; Jaravine et al. 2006; Jeong et al. 1993; Jiang et al. 2010; Kim and Szyperski 2003; Kupce and Freeman 2003; Laue et al. 1985; Malmodin and Billeter 2006; Mandelshtam et al. 1998; Matsuki et al. 2009; Shrot and Frydman 2011; Sibisi et al. 1984; Zhang and Bruschweiler 2004). These methods allow for different degrees of linearity between time- and frequency-domain signals and pose different requirements for the data quality (e.g., degree of sparseness, signal-to-noise ratio etc.). We have recently introduced an approach dubbed maximum entropy interpolation (MINT) where entropy maximization is used to estimate the values of missing data samples, while tightly constraining the resulting spectrum to closely match the measured samples based on the NUS sampling schedule (Paramasivam et al. 2012). As we have demonstrated, MINT ensures highly linear time- to frequency-domain transformation, permitting direct assessment of the NUS-based sensitivity gains in the frequency domain of multidimensional MAS NMR spectra. While careful analysis conducted in our previous study led us to conclude that inherent time-domain sensitivity enhancements as high as twofold are attained in each indirect dimension due to NUS alone and without compromising line widths, the original work was conducted on heteronuclear datasets possessing relatively limited dynamic range.

Here, we extend our initial studies to multidimensional MAS NMR spectra of high dynamic range, and report that under these more stringent conditions, both the sensitivity gains and the linearity of the time–frequency domain transformation are attained under NUS/MINT. For this purpose, we selected homonuclear ^{13}C–^{13}C correlation experiments characterized by dynamic range as high as 245 under our experimental conditions. We demonstrate that the NUS/MINT approach results in high fidelity spectra from datasets of both high and low inherent sensitivity, model compounds and a protein, 1–73-(U-^{13}C,^{15}N)/74–108-(U-^{15}N) *E. coli* thioredoxin reassembly, respectively. We discuss our approach to creating NUS schedules that result in high-quality datasets exhibiting 1.7–2.0 fold inherent sensitivity enhancement without compromising on the linearity or the line widths. We demonstrate that both the peak positions and spectral intensities are highly reproducible by NUS/MINT, repeating the same experiments multiple times under identical acquisition and processing conditions. Furthermore, we show that the sensitivity and line widths of the NUS datasets do not correlate with the peak position or intensity, and uniform linear behavior is retained throughout the entire dynamic range. Taken together, our results attest to the excellent

potential of NUS/MINT approach for accelerating MAS NMR data collection and obtaining reliable frequency and intensity information from various kinds of datasets. We anticipate that NUS/MINT can be used for a wide variety of MAS solid-state NMR correlation experiments to increase sensitivity for the studies of interesting and challenging biological systems.

Experiments and methods

Materials

U-$^{13}C_6$-glucose and $^{15}NH_4Cl$, as well as the tri-peptide MLF were purchased from Cambridge Isotope Laboratories (Andover, MA, US), and used without further purification. U-^{13}C, ^{15}N L-histidine was purchased from Cambridge Isotope Laboratories and was doped with 0.1 mol% $CuCl_2$ and recrystallized before use. The media used for *E. coli* cultures of 1–73-(U-^{13}C,^{15}N)/74–108-(U-^{15}N) reassembled thioredoxin was purchased from Oxoid, Inc. (Nepean, ON, CA).

Solid-state NMR sample preparation

Approximately 3 mg (ca. 7 μmol) of powdered MLF were packed into a 1.6 mm Varian MAS rotor and sealed with a spacer and spinner for data collection at the University of Delaware. Another MLF sample was packed into a 3.2 mm Varian MAS rotor and sealed with a spacer and spinner for data collection at the Environmental Molecular Sciences Laboratory (EMSL).

Approximately 12.0 mg (57.4 μmol) of U-^{13}C, ^{15}N L-histidine recrystallized with 0.1 mol% $CuCl_2$ was packed into a 1.8 mm MAS rotor and sealed with a spacer and top spinner and used for data collection at the University of Delaware.

The 1–73-(U-^{13}C,^{15}N)/74–108-(U-^{15}N) reassembled thioredoxin sample was prepared by controlled precipitation as described previously (Marulanda et al. 2004, 2005; Yang et al. 2007, 2008, 2009); 11 mg of 1–73(U-^{13}C,^{15}N)/74–108(U-^{15}N) reassembled thioredoxin were packed into a 3.2 mm Varian MAS rotor and sealed with a spacer and spinner.

NMR spectroscopy

Solid-state NMR spectra of MLF were acquired both at the University of Delaware and at the Environmental Molecular Sciences Laboratory (EMSL). Experiments for L-histidine and 1–73(U-^{13}C,^{15}N)/74–108(U-^{15}N) thioredoxin reassembly were performed at the University of Delaware.

At the University of Delaware, a 14.1 T narrow bore Varian InfinityPlus spectrometer operating at Larmor frequencies of 599.8 (^{1}H), 150.8 (^{13}C) and 60.8 (^{15}N) MHz was used for all data collection. For MLF, a 1.6 mm Varian NB HXY FastMAS probe was utilized. For L-histidine, a 1.8 mm triple-resonance probe developed in the laboratory of Ago Samoson (Tallinn University of Technology, Tallinn, Estonia) was used. Experiments for 1–73(U-^{13}C,^{15}N)/74–108(U-^{15}N) reassembled thioredoxin were conducted using a 3.2 mm Varian triple-resonance T3 HXY probe. The MAS frequencies for each experiment were set to 10 kHz and controlled to ±2 Hz by a Varian MAS controller.

At EMSL, a 21.1 T Agilent VNMRS spectrometer operating at Larmor frequencies of 900.3 (^{1}H), 226.4 (^{13}C), and 91.2 (^{15}N) MHz was used; the instrument is equipped with a 3.2 mm BioMAS HXY probe. The MAS frequency was set to 14 kHz and controlled to ± 1 Hz by an Agilent MAS controller.

Two-dimensional US 14.1 T ^{13}C–^{13}C DARR (Takegoshi et al. 2001) spectra of MLF were collected at the University of Delaware as a (2,000 × 1,024) complex matrix with four scans per t_1 increment. Two-dimensional NUS DARR spectra of MLF were acquired as a (2,000 × 512) complex matrix with eight scans per t_1 increment. The dwell time was 33.33 μs in the case of both US and NUS sampled data. For US spectra, the 1,024 t_1 increments were equally spaced by the dwell time until the final evolution time of 34.1 ms. For the two NUS spectra, the 512 t_1 points were distributed in an exponentially weighted manner, adhering to decay rates of either 35 Hz (based on the T_2* of slowest decaying signal) or 100 Hz (based on the average T_2*'s of the signals in the sample) with the final sampled data point (corresponding to point 1,024 in the US dataset) being sampled at 34.1 ms. In all cases, the total experiment times were equivalent.

Two-dimensional US selective ^{13}C–^{13}C DARR spectra of MLF were collected at EMSL as a (1,000 × 512) complex matrix with 16 scans per t_1 increment. Two-dimensional NUS selective ^{13}C–^{13}C DARR spectra of MLF were collected as a (1,000 × 256) complex matrix with 32 scans per t_1 increment. The dwell time was 59 μs in the case of both US and NUS sampled data. For US spectra, the 512 t_1 increments were equally spaced by the dwell time until the final evolution time of 30.1 ms. For NUS spectra, the 256 t_1 points were distributed in an exponentially weighted manner while adhering to a decay rate of 125 Hz with the final sampled data point (corresponding to point 512 in the US dataset) being sampled at 30.1 ms. In both cases, the total experiment time was equivalent.

The two-dimensional US ^{13}C–^{13}C DARR spectrum of L-histidine was collected as (1,000 × 320) complex matrices

with 16 scans per t_1 increment. Ten two-dimensional NUS DARR spectra of L-histidine were collected as (1,000 × 160) complex matrices with 32 scans per t_1 increment. The dwell time was 33.33 μs in the case of both US and NUS sampled data. For US spectra, each of the 320 t_1 points were equally spaced by the dwell time until the final evolution time of 10.6 ms. For the ten NUS spectra, the 160 t_1 points were distributed in an exponentially weighted manner adhering to a decay rate of 230 Hz with the final sampled data point (corresponding to point 320 in the US dataset) being sampled at 10.6 ms. The same NUS experiment was repeated 10 times for L-histidine to gauge the reproducibility of the results.

Additional experiments for L-histidine were collected using (1) a 50 % NUS schedule with 16 scans (equivalent number of scans to the US datasets) where 50 % of the experiment time is saved, (2) a 25 % NUS schedule with 16 scans (equal to the US experiment) where 75 % of the experiment time is saved compared to the US collected data. The 50 % NUS experiment collected with the number of scans equal to the US experiment was a (1,000 × 160) complex matrix with a dwell time set at 33.33 μs. The 160 t_1 points were distributed according to the same 50 % NUS schedule described above (based on a 230 Hz decay rate). The 25 % NUS experiments, where 75 % of the experiment time was saved compared to US, were acquired as (1,000 × 80) complex matrices with a dwell time set to 33.33 μs. The 80 t_1 increments were distributed according to a NUS schedule based on a 230 Hz decay rate, and the final data point was sampled at the evolution time of 10.6 ms (corresponding to point 320 in the US dataset). In addition to these equivalent time experiments, sub-sampled US datasets were created and assessed by removing points from the uniformly sampled experiment of L-histidine based on NUS sampling schedules corresponding to 90, 80, 70, 60, 50, 40, 30, 25, 20, 10, and 5 % sampling schedules. The sampling schedules used for this assessment were designed based on a 230 Hz decay rate.

Two-dimensional US ^{13}C–^{13}C DARR spectra of 1–73(U-^{13}C,^{15}N)/74–108(U-^{15}N) reassembled thioredoxin were collected as a (1,000 × 512) complex matrix with 16 scans per t_1 increment. Two-dimensional NUS DARR spectra of 1–73(U-^{13}C,^{15}N)/74–108(U-^{15}N) reassembled thioredoxin were collected as a (1,000 × 256) complex matrix with 32 scans per t_1 increment. The dwell time was 33.33 μs for both US and NUS datasets. For US spectra, the 512 t_1 increments were equally spaced by the dwell time until the final evolution time of 17.0 ms. For NUS spectra, the 256 t_1 points were distributed in an exponentially weighted manner according to a decay rate of 100 Hz with the final sampled data point being sampled at 17.0 ms.

In all experiments, the $3T_2^*$ limit was satisfied for the overwhelming majority of the peaks in the samples under study, to attain maximum resolution and maximum enhancement (Paramasivam et al. 2012; Rovnyak et al. 2011). The NUS schedules were constructed using a NUS scheduler program (http://sbtools.uchc.edu/nmr/sample_scheduler/).

NMR data processing and analysis

All spectra were processed using the RNMRTK (http://rnmrtk.uchc.edu) software package and then analyzed using SPARKY3 (Goddard and Kneller 2004).

In all datasets, FFT was used to process the directly detected dimensions (acquired uniformly), while the indirect dimensions (both US and NUS) were processed by MINT in RNMRTK. As discussed in our previous work, and shown in figure S1, of the supporting information, equivalent results are obtained when the same US dataset is processed with FFT and MINT (Hoch and Stern 1996). Additional acquisition and processing details can be found in the Supporting Information.

The analytical expressions for calculating the expected inherent sensitivity enhancements in NUS experiments have been reported by us previously (Paramasivam et al. 2012; Rovnyak et al. 2011). We reiterate these here for the convenience of the reader.

The enhancement of the SNR in the time domain is as follows:

$$\eta = \frac{\chi\left(1 - e^{-\alpha(T_2/T_{\mathrm{SMP}})+1}\right)}{(T_2/T_{\mathrm{SMP}} + 1)(1 - e^{-\alpha})} \quad (1)$$

where scaling factor χ is such that the areas under the uniform and NUS sampling density curves are equal (Rovnyak et al. 2011):

$$\eta = \frac{\alpha(T_2/T_{\mathrm{SMP}})}{(1 - e^{-\alpha T_2/T_{\mathrm{SMP}}})}, \quad (2)$$

where T_{SMP} is the exponential decay constant for the sampling density, and the evolution is parameterized by T_2^* via $\alpha = t_{max}/T_2$. If $S(t) = e^{-t/T_2}$ is the uniformly sampled FID scaled by unity, the NUS-scaled FID, which consumes the identical experimental time, is given by $\chi S(t)$.

Results and discussion

Sensitivity, line widths, and decay rate of NUS schedules

To test the extent to which the NUS/MINT approach can accurately reconstruct data over a broad dynamic range spanning two orders of magnitude, we performed ^{13}C–^{13}C DARR experiments on the tripeptide MLF. We tested two

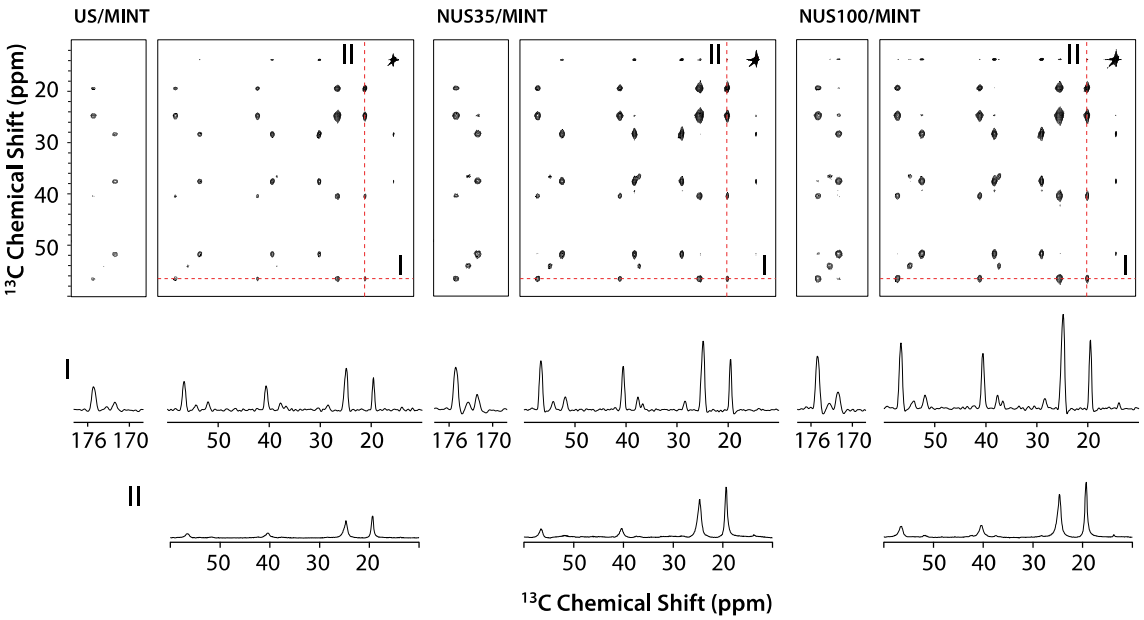

Fig. 1 A comparison of the 2D DARR spectra of U-^{13}C,^{15}N-MLF collected with a full spectral width: US/MINT (*left*), NUS35/MINT (*middle*), and NUS100/MINT (*right*). One-dimensional traces through the direct (*I*) and indirect (*II*) dimensions show a clear increase in peak intensity for the NUS datasets displayed at the same contour level. In all cases the RMS noise was found to be equivalent to within 2.4 % error and was measured over 65,534 points in a signal-free region of the spectra. The US dataset was collected as a (2,000 × 1,024) complex matrix with four scans per t_1 increment. NUS35 and NUS100 were collected as a (2,000 × 512) complex matrix with eight scans per t_1 increment. NUS35 was collected with a schedule based on a 35 Hz decay rate whereas NUS100 was collected with a schedule based on a 100 Hz decay rate. The datasets possess a dynamic range spanning two orders of magnitude

different exponentially weighted NUS schedules, characterized by 35 and 100 Hz decay rates, which correspond to the longest T_2* (observed for the MC_δ–MC_δ diagonal peak) and to the average T_2* in the sample. We refer to these schedules as NUS35 and NUS100, respectively. In both cases, the indirect dimension was sampled to the final evolution time of 34.1 ms, which exceeds the $3T_2^*$ limit for all coherences in the sample other than the MC_δ–MC_δ signal. In Fig. 1, a comparison of the 2D DARR spectra is shown for the US/MINT, NUS35/MINT, and NUS100/MINT datasets along with representative 1D traces extracted from the direct and indirect dimensions. In all three cases the experiment time was identical.

The linearity of the above two NUS/MINT datasets with respect to the US/MINT spectrum can be assessed directly, as we reported previously (Paramasivam et al. 2012). The relative peak intensity in a given dataset is taken as the ratio between the intensity of each peak over that of a representative strong peak in the same dataset. In our datasets, we use the LC_δ–LC_δ correlation as the intensity marker. In Fig. 2a, the peak intensities for the NUS35 and NUS100 datasets are plotted relative to those of the US spectra. As is obvious from the figure, a highly linear correlation is retained throughout the entire dynamic range. For NUS35, the errors in the slope and the y-intercept are 2.9 and 1.7 %, respectively. The R^2 value for the data is equal to 0.994. In the case of NUS100, the errors in the slope and the y-intercept are 1.5 and 0.14 %, respectively; the R^2 value is equal to 0.999.

To assess the inherent sensitivity enhancements, the relative peak intensities in the NUS/MINT and the US/MINT spectra can be compared directly, provided that the noise RMS levels in the frequency domain are equivalent (Paramasivam et al. 2012). This requirement is attained in the current datasets, where the RMS of the noise is 15.6 (US), 15.6 (NUS35), and 16.0 (NUS100), as measured by a signal-free region of the spectra containing 65,534 samples. Analysis of relative peak intensities in these datasets is summarized in Table 1 and reveals that the inherent sensitivity enhancements, on average, are 1.69- and 2.11-fold for NUS35 and NUS100, respectively. These findings are in line with our prior observations on the inherent sensitivity enhancements in heteronuclear datasets (Paramasivam et al. 2012). It is interesting to note the variation of the degree of signal enhancement in both datasets: the range is 1.25–1.97 and 1.79–2.38 fold for NUS35 and NUS100, respectively. Importantly, there is no correlation between the absolute peak intensity (or the signal position) and the degree of sensitivity enhancement, that is, weak and strong peaks are enhanced to a similar degree. Figure S2 of the Supporting Information shows a scatter plot of absolute peak intensity versus inherent sensitivity

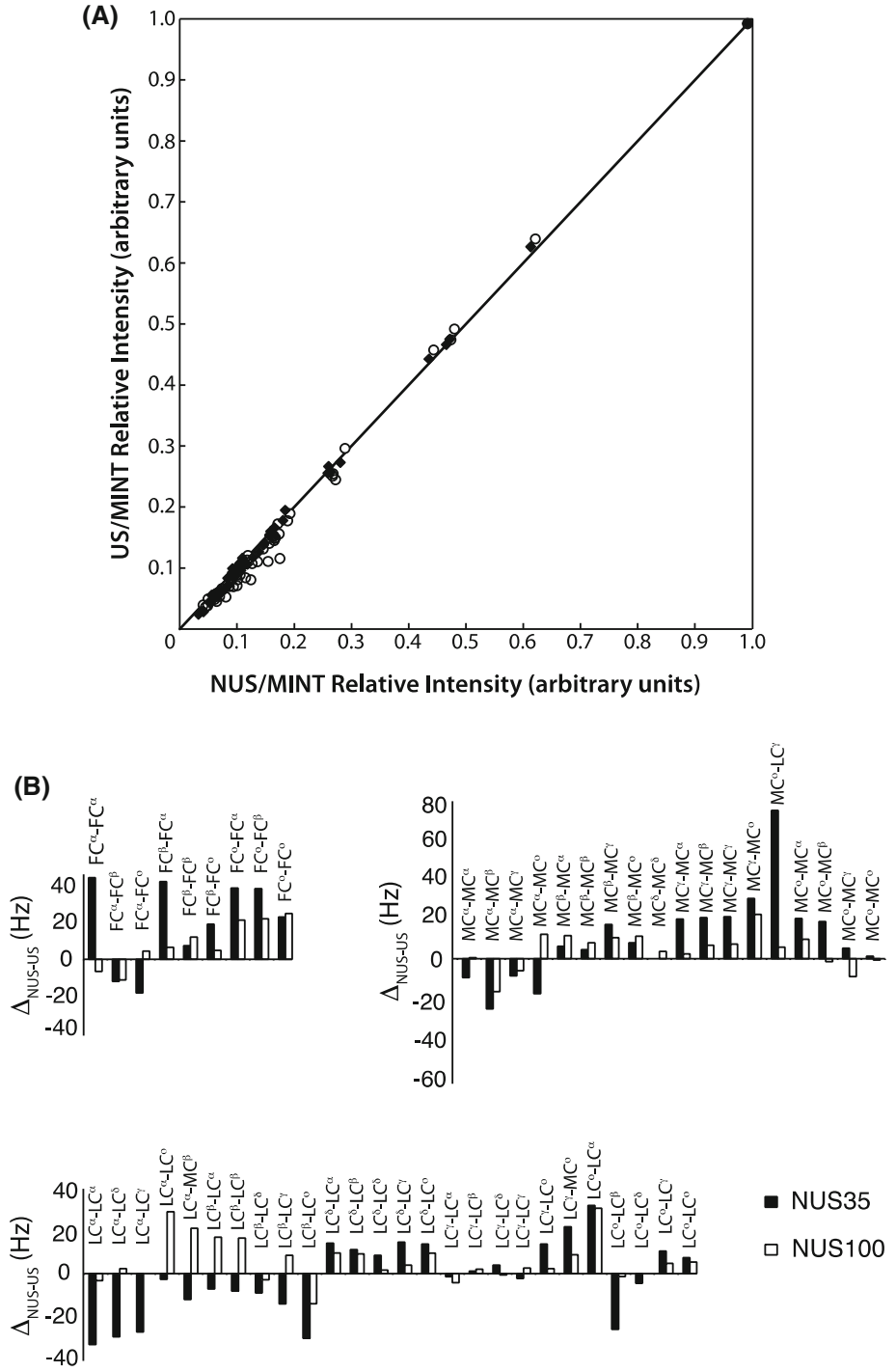

Fig. 2 **a** Correlation plot of the relative cross-peak intensities in 2D DARR spectra of U-^{13}C,^{15}N-MLF (with a full spectral width) collected and processed as US/MINT, NUS35/MINT (*white circles*), and NUS100/MINT (*black diamonds*). High linearity is attained by MINT transformation, in line with our previous studies[16]. The slopes are 1.029 (2.9 % error) and 1.015 (1.5 % error) for NUS35 and NUS100, respectively. The y-intercepts are 0.017 (1.7 % error) for NUS35 and 0.0014 (0.14 % error) for NUS100. The R^2 values are 0.994 and 0.999 for NUS35 and NUS100, respectively. **b** Comparison of the line width differences in the indirect dimension of the full spectral width DARR spectra for residues F (*top*), L (*middle*), and M (*bottom*) collected as NUS35/MINT (*black*) and NUS100/MINT (*grey*). All data were processed under identical conditions; the resulting RMS noise level is equivalent for the two datasets within 2.4 % error. The noise levels were measured using a signal-free region of the spectra containing 14,542 samples. On average, the line widths are greater by 5.5 and 5.9 % in the NUS35/MINT and NUS100/MINT datasets, respectively with respect to the US/MINT spectrum. Arbitrary units used for normalization

Table 1 Inherent sensitivity enhancement for the NUS 2D DARR spectra of MLF

Correlation	NUS35/MINT sensitivity enhancement	NUS100/MINT sensitivity enhancement	Correlation	NUS35/MINT sensitivity enhancement	NUS100/MINT sensitivity enhancement
FCα–Cα	1.47	2.03	LCγ–Cγ	1.92	2.11
FCα–Cβ	1.53	1.95	LCγ–Co	1.72	2.09
FCα–Co	1.66	2.05	LCγ–MCo	1.91	1.79
FCβ–Cα	1.50	1.89	LCo–Cα	1.68	2.12
FCβ–Cβ	1.71	1.95	LCo–Cβ	1.75	2.29
FCβ–Co	1.54	1.98	LCo–Cδ	1.72	2.12
FCo–Cα	1.69	2.12	LCo–Cγ	1.70	2.25
FCo–Cβ	1.66	2.12	LCo–Co	1.82	2.23
FCo–Co	1.88	2.26	MCα–Cα	1.68	2.15
LCα–Cα	1.53	2.11	MCα–Cβ	1.72	2.19
LCα– Cδ	1.40	2.02	MCα–Cγ	1.71	2.20
LCα– Cγ	1.38	2.07	MCα–Co	1.63	2.00
LCα–Co	1.55	1.92	MCβ–Cα	1.72	2.12
LCα–MCβ	1.42	1.93	MCβ–Cβ	1.80	2.13
LCβ–Cα	1.25	2.03	MCβ–Cγ	1.72	2.10
LCβ–Cβ	1.36	2.11	MCβ–Co	1.56	2.04
LCβ–Cδ	1.25	2.06	MCδ-Cδ	1.85	2.10
LCβ–Cγ	1.27	1.99	MCγ–Cα	1.93	2.11
LCβ–Co	1.35	1.97	MCγ–Cβ	1.97	2.10
LCδ–Cα	1.73	2.03	MCγ–Cγ	1.96	2.15
LCδ–Cβ	1.80	2.15	MCγ–Co	1.94	2.10
LCδ–Cδ	1.97	2.18	MCo–LCγ	1.85	1.96
LCδ–Cγ	1.98	2.17	MCo–Cα	1.86	2.17
LCδ–Co	1.61	2.02	MCo–Cβ	1.81	2.27
LCγ–Cα	1.88	2.29	MCo–Cγ	1.79	2.38
LCγ–Cβ	1.82	2.21	MCo–Co	1.84	2.33
LCγ–Cδ	1.92	2.14			

The spectra were acquired with a full spectral width. The inherent sensitivity enhancements were obtained for two NUS schedules: NUS35 matched to the exponential decay rate of 35 Hz, and NUS100 matched to the exponential decay rate of 100 Hz. These enhancements are measured as intensity ratios defined with respect to the corresponding US spectrum collected with the same experiment time and processed using MINT with identical settings (the noise RMSD are equivalent to within 2.4 % as measured in the frequency domain)

enhancement factor for NUS35 and NUS100 datasets. The degree of intensity enhancement is more uniform in NUS100, which is not surprising given the fact that this schedule was exponentially weighted to the decay rate of the majority of the signals in the sample while NUS35 is biased toward the longest-decaying peak. The lack of correlation between the absolute signal intensity and the degree of enhancement is a very important finding attesting to the utility of absolute peak intensities in the NUS/MINT spectra for derivation of quantitative spectral information.

We next examined whether the variations in the inherent sensitivity enhancements discussed above originate from the different T_2* values across the sample. The relative enhancements have been shown theoretically to correlate with the T_2*, see Eqs. 1 and 2 (Paramasivam et al. 2012; Rovnyak et al. 2011). Our analysis of the experimental results revealed that indeed, the relative enhancements exhibit monotonic dependence on the T_2* in MLF, as shown in Fig. 3. This result is an illustration of the fact that the variations in the relative signal enhancements in the NUS experiments are not random but are due to the spread in T_2* values across the sample. The dependence of the enhancements on T_2*/T_{SMP} values will be investigated more thoroughly in the future.

It is also instructive to assess the line widths across the three datasets by comparison of the width of the individual cross peaks in the spectra. This analysis reveals that the peaks in both NUS datasets are slightly broader than in the US spectrum: the average line widths in NUS35 and NUS100 datasets are greater by 5.6 and 6.0 Hz, or by 5.5 and 5.9 % than in the US spectrum. These values are consistent with our earlier findings for the heteronuclear

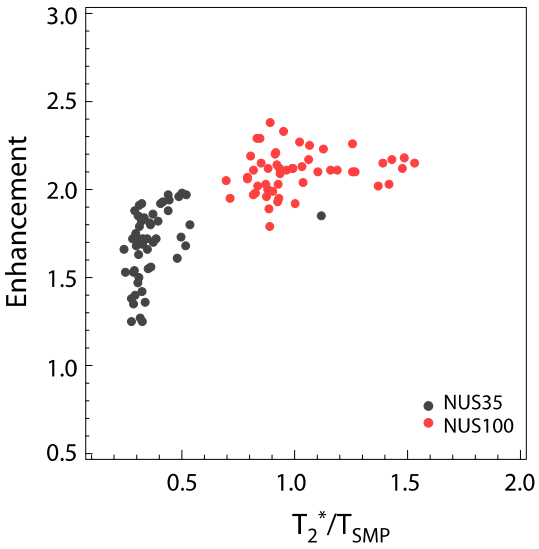

Fig. 3 Sensitivity enhancements in NUS data for two sampling schedules NUS35 (*dark grey*) and NUS100 (*red*) plotted as a function of the apparent spin–spin relaxation times T_2* normalized by the exponential decay constant for the sampling density T_{SMP}. The experimental data points were extracted from the 2D DARR spectra of U-^{13}C,^{15}N-MLF (see Fig. 1)

NUS datasets. Interestingly, there is a variation in the line widths: for NUS35, the differences in the line widths with respect to US range from −35.1 to 40.4 Hz, while in NUS100—from 16.3 to 32.4 Hz. These results are summarized in Fig. 2b and Figure S3 of the Supporting Information. Importantly, there is no correlation between the difference in line widths and the absolute peak intensity. The NUS100 dataset shows a tighter range of the values for the difference in line widths, in line with the observation for the relative sensitivity enhancement and likely a reflection of the exponential weighting being tailored to the decay rates of the majority of the coherences in the spectra, as discussed above.

We note that in spectra of proteins and protein assemblies the distribution of T_2* values is usually narrow enough to permit constructing NUS schedules that would be optimal for the majority of the peaks in the sample. Nevertheless, rigorous analysis of the general dependence of sensitivity enhancement factors on the line widths for different sampling schedules is necessary and will be conducted in the future using samples that possess a wide range of T_2* values.

Spectral width

Another important practical consideration is the influence of the spectral width on the quality of the NUS datasets. ^{13}C signals span a range of 200 ppm, and therefore sampling the entire spectral width in the indirect dimensions of homonuclear correlation spectra requires short dwell times, which also means that sampling to long evolution times is often impractical. For instance, in the MLF conventional DARR spectra acquired at 14.1 T, we could not sample in the indirect dimension to the $3*T_2^*$ limit for the longest-decaying signal MC_δ–MC_δ because of the prohibitively large number of t_1 points that would be required due to the large spectral width (and correspondingly short dwell time). We therefore had to exclude this peak from the analysis of spectral linearity. Since MC_δ–MC_δ, is the strongest peak in the spectra, its omission also reduced the effective dynamic range used in the data analysis. To include this peak into consideration and to attain the required evolution times within reasonable total experiment times, we have reduced the spectral width in the indirect dimension by conducting a bandwidth-selective DARR experiment where excitation of the aliphatic region only is performed, and the spectral width is reduced by a factor of two in the indirect dimension. These experiments were performed at 21.1 T at EMSL. Under the experimental conditions attained at EMSL, the $3T_2^*$ limit for this longest-decaying peak is well exceeded by sampling to an evolution time of 30.1 ms. This experimental setting permits us to exploit the full two orders of magnitude dynamic range in the data analysis.

In Fig. 4, the 2D planes are displayed together with the selected 1D traces for the US and NUS selective DARR spectra. Note that for the equivalent experiment times, the NUS spectrum exhibits additional cross peaks that are not present in the US dataset due to the limited sensitivity of the latter. Similar to the 14.1 T NUS DARR spectra acquired with the full spectral width, the 21.1 T selective NUS DARR spectrum attains excellent linearity with respect to the corresponding US datasets. The slope for the data is 1.0014 (0.14 % error) with a y-intercept of +0.0004 (0.04 % error). Figure 5 displays the correlation plot for the full dynamic range (A) and an expansion around the region highlighting the majority of the signals (B). Most of the correlations fall on or near the straight line with very little scatter.

For this selective ^{13}C–^{13}C DARR experiment, the average inherent sensitivity enhancement was found to be 1.91 fold. The RMS noise levels as determined in the frequency domain by measuring a signal-free region of the spectra containing 53,248 samples are 10.9 and 11.2 for the US and NUS collected datasets respectively (2.8 % error). The range of sensitivity enhancement for the various peaks in the spectrum is 1.71–2.11 fold, and there is no correlation between the sensitivity enhancement factor and the absolute peak intensity, as illustrated in Figure S2 of the Supporting Information. These results are summarized in Table 2.

The analysis of line widths in the selective DARR NUS dataset reveals that, on average, the peaks are only 1.9 Hz

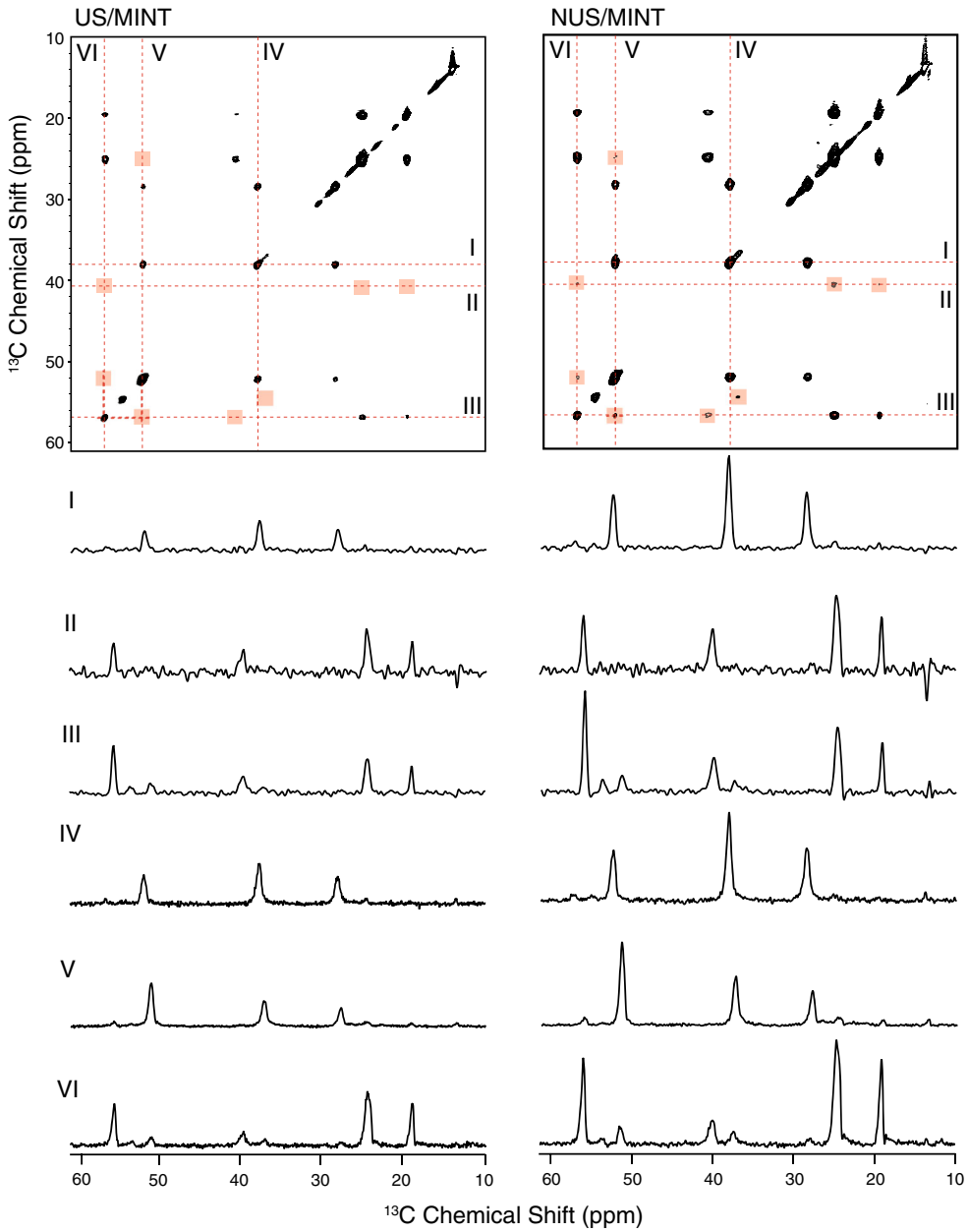

Fig. 4 A comparison of the 2D selective DARR experiment of U-^{13}C,^{15}N-MLF collected and processed with US/MINT (**a**) and NUS/MINT (**b**). Slices are shown through the direct (*I*, *II*, *III*) and indirect (*IV*, *V*, *VI*) dimensions. In both cases the RMS noise measured over 53,284 points in a signal-free region of each frequency domain spectrum is equivalent within 3.2 %. *Pink boxes* display regions where peak intensities are present in the NUS and not in the US data when displayed at an equivalent contour level. The US dataset was collected as a (1,000 × 512) complex matrix with 16 scans per t_1 increment. The NUS/MINT dataset was collected as a (1,000 × 256) complex matrix with 32 scans per t_1 increment. The NUS schedule used for the collection of this dataset was based on a 125 Hz exponential decay. For these datasets the observed dynamic range was ∼245×

(1.5 %) broader than in the corresponding US spectrum, and the differences in line widths vary from −25.8 Hz to 38.6 Hz. Again, there is no correlation between the line widths and the absolute peak intensities while the line widths do correlate with the relative signal enhancements, in agreement with theory and the discussion above, and indicating that NUS spectra can be used to reliably quantify the spectral parameters. These results are illustrated in Figs. 5C and S3 of the Supporting Information.

Reproducibility of spectral features in the NUS datasets

Another important consideration is how reproducible the features in the NUS/MINT datasets are from experiment to

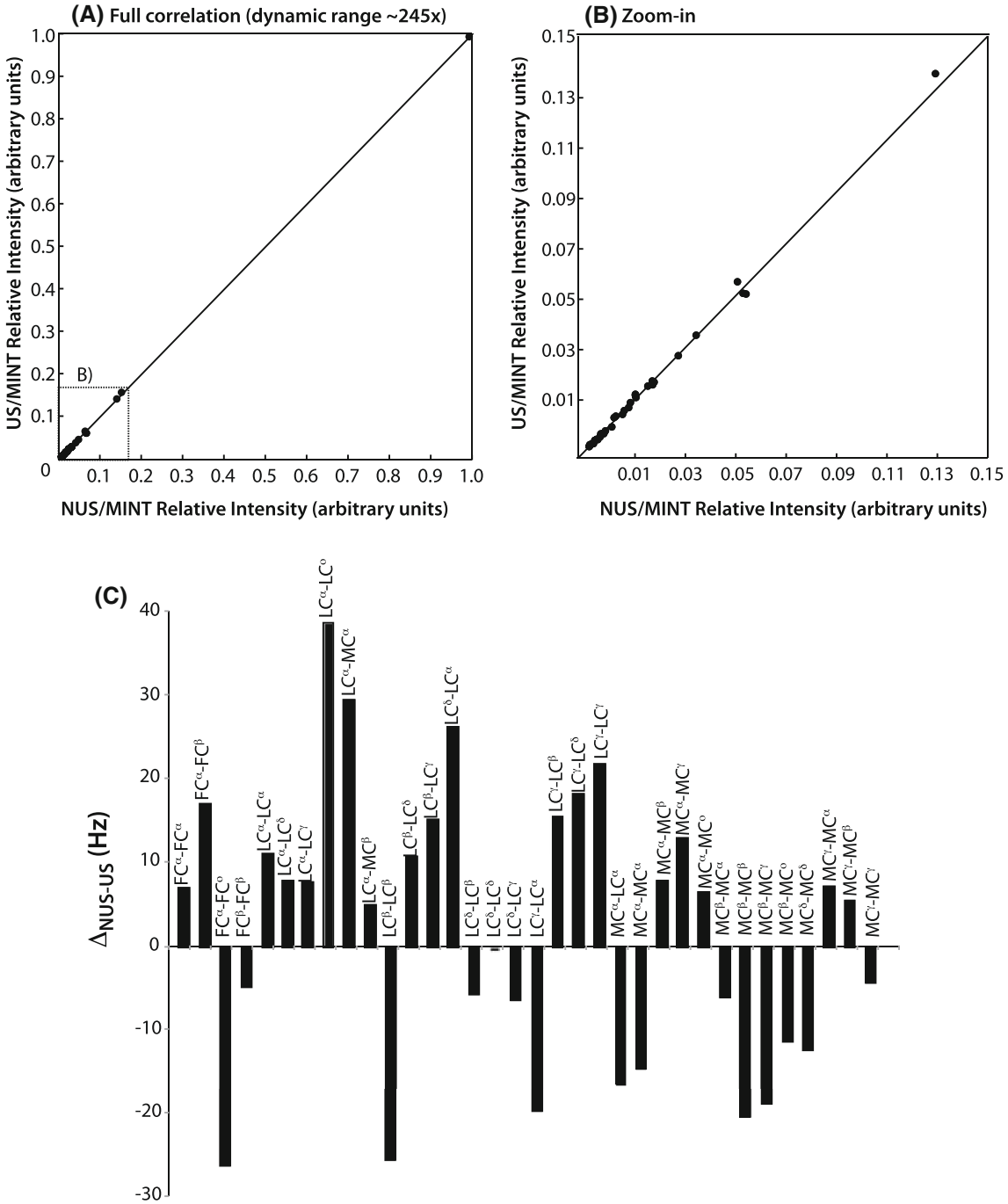

Fig. 5 A correlation plot of the relative cross-peak intensities for the selective 2D DARR spectra of U-^{13}C,^{15}N-MLF collected and processed as US/MINT and NUS/MINT shown over the full dynamic range of ~245× (**a**) and zoomed in **b** to highlight the majority of the signals. The linearity between these two datasets is remarkably good. The slope 1.0014 (0.14 % error) and the y-intercept is 0.0004 (0.04 % error). The R^2 value for the data is 0.999. **c** Comparison of the line width differences in the indirect dimension of the selective DARR spectra collected with NUS/MINT–US/MINT (*black*). All data were processed under identical conditions; the resulting RMS noise level is equivalent within 3.2 %, as measured in a signal-free region of the frequency domain spectra containing 65,534 samples. On average, the line widths in the NUS/MINT are broader by a modest 1.92 Hz (1.52 %). Arbitrary units used for normalization

experiment, and in particular how well the linearity, the inherent sensitivity enhancements, and the peak line widths can be reproduced in multiple measurements. To assess this, we repeated the DARR experiments ten times using the same sampling schedule, experimental setup, and processing scripts and following the same protocols outlined

Table 2 Inherent sensitivity enhancement for the NUS 2D selective DARR spectra of MLF

Correlation	NUS/MINT sensitivity enhancement	Correlation	NUS/MINT sensitivity enhancement
FCα–Cα	1.90	LCγ–Cα	1.92
FCα–Cβ	1.73	LCγ–Cβ	1.96
FCα–Co	1.97	LCγ–Cδ	1.85
FCβ–Cβ	1.97	LCγ–Cγ	1.99
LCα–Cα	2.06	MCα–LCα	2.11
LCα–Cδ	1.71	MCα–Cα	1.92
LCα–Cγ	2.07	MCα–Cβ	1.93
LCα–Co	1.87	MCα–Cγ	1.82
LCα–MCα	1.90	MCα–Co	1.84
LCα–MCβ	1.78	MCβ–Cα	1.91
LCβ–Cα	1.95	MCβ–Cβ	1.89
LCβ–Cβ	1.92	MCβ–Cγ	1.82
LCβ–Cδ	1.93	MCβ–Co	1.73
LCβ–Cγ	1.75	MCδ–Cδ	1.90
LCδ–Cα	2.02	MCγ–Cα	1.84
LCδ–Cβ	2.05	MCγ–Cβ	1.85
LCδ–Cδ	2.04	MCγ–Cγ	1.81
LCδ–Cγ	2.04		

The inherent sensitivity enhancements are measured as intensity ratios defined with respect to the corresponding US spectrum collected with the same experiment time and processed using MINT with identical settings (the noise RMSD's are equivalent to within 3.2 % as measured in the frequency domain). The NUS schedule is matched to a 125 Hz exponential decay

above and in our previous report (Paramasivam et al. 2012). The U–^{13}C–^{15}N L-histidine sample was employed for this purpose. In addition, using sub-sampled US datasets, we addressed the spectral variability resulting from 50 % sampling schedules created using different random seeds to generate the NUS schedules.

The results for the ten experiments collected using the same sampling schedule are summarized in Table 3 and Figure S4, where the relative peak intensities in the NUS datasets are plotted versus those in the US spectrum for the ten measurements. It is obvious that the results are fully consistent between the different datasets, and the spectral linearity is excellent. The average slope is 1.014 (1.4 % error) with values ranging from 1.004 (0.44 % error) to 1.024 (2.4 % error). The average y-intercept is −0.0095 (0.95 % error) with values ranging from −0.008 (0.8 % error) to −0.011 (1.1 % error). The average R^2 is 0.990 with values ranging from 0.991 to 0.988.

The average sensitivity enhancement for all cross peaks in the ten NUS experiments using the same sampling schedule is 1.90 fold, completely in line with the datasets discussed in the previous sections. The average values range between 1.88 and 1.92 fold over the ten experiments, with the largest difference between any two datasets being only 2 %. As for other datasets, there is no correlation between the degree of signal enhancement and the absolute peak intensity, as illustrated in Figure S2 of the Supporting Information.

Interestingly, for this sample we observe that the line widths are narrowed on average for the NUS dataset compared to the US spectrum: the average difference in line width in the indirect dimension amongst the ten datasets is −1.5 Hz with values ranging from −2.1 to 0.4 Hz. Again, there is no correlation between the difference in peak width and the absolute signal intensity, while the peak widths and the relative signal enhancements do correlate, as discussed above. The results are summarized in Table 3, and in Figure S3 and Tables S1–S10 of the Supporting Information.

The results for the sub-sampled US datasets generated from sampling schedules created with different random seeds are summarized in Figure S5 and Table S11. As expected, the variation in spectral properties is somewhat greater between these datasets than that seen for the ten experiments collected with the same NUS sampling schedule. Nonetheless, the data display good linearity. The average slope is 0.994 (0.6 %) with values ranging from 0.944 (5.6 % error) to 1.050 (5 % error). The average y-intercept is 0.008 (0.8 % error) with values ranging from −0.03 (3 % error) to +0.01 (1 % error). The average R^2 is 0.988 with values ranging from 0.973 to 0.997.

The average sensitivity enhancements for all cross peaks is 1.33 fold, which is 6.3 % less than that expected theoretically for removal of 50 % of the points, compared to a uniformly sampled grid. The enhancement values range from 1.27 fold (11.3 % error) to 1.39 fold (1.7 %).

Taken together, the data collected with the same sampling schedules confirm our previous finding that the MINT transformation is highly reproducible and shows deviations only within the instrumental noise level. In addition, the sub-sampled data show that although there are small variations in the linearity and enhancement properties for data collected with sampling schedules created with different random seeds, the results are still in reasonable agreement and make NUS a robust method for collection of multidimensional solid-state NMR datasets.

How sparse can a NUS schedule be?

In our NUS experiments, we have adopted a conservative approach by removing only 50 % of the points in the indirect dimension, which were compensated for by doubling the number of scans. To test how sparse a NUS schedule could be while maintaining adequate linearity we have conducted the following additional analysis. First, we

Table 3 Average inherent sensitivity enhancement and line width properties for NUS DARR spectra of L-histidine

Correlation	NUS/MINT average sensitivity enhancement (lowest, highest amongst 10 experiments)	Line width (lowest, highest values amongst 10 experiments)	Correlation	NUS/MINT average sensitivity enhancement (lowest, highest amongst 10 experiments)	Line width (lowest, highest values amongst 10 experiments)
Cα–Cα	1.88 (1.87, 1.89)	−3.3 (−5.5, 0)	Cε–Cα	1.97 (1.95, 1.98)	+0.8 (−8.6, +12.7)
Cα–Cβ	1.84 (1.81, 1.86)	−3.6 (−5.9, −1.9)	Cε–Cβ	1.96 (1.94, 1.98)	+6.2 (−5.6, +27.5)
Cα–Cδ	1.79 (1.75, 1.82)	−10.0 (−13.3, −6.5)	Cε–Cδ	1.96 (1.92, 2.00)	+0.1 (−9.9, +13.2)
Cα–Cε	1.80 (1.78, 1.81)	−7.7 (−15.6, −3.1)	Cε–Cε	1.97 (1.91, 2.00)	−3.5 (−12.1, +4.1)
Cα–Cγ	1.70 (1.67, 1.73)	−4.4 (−6.7, +3.7)	Cε–Cγ	1.96 (1.88, 1.98)	−12.8 (−24.0, +5.0)
Cα–Co	1.89 (1.87, 1.91)	−4.7 (−12.4, −0.7)	Cε–Co	1.95 (1.92, 1.98)	−2.0 (−9.6, +9.9)
Cβ–Cα	1.98 (1.95, 2.00)	−9.1 (−12.6, −1.9)	Cγ–Cα	1.70 (1.66, 1.72)	−4.5 (−9.5, +1.1)
Cβ–Cβ	1.95 (1.92, 1.97)	−9.2 (−11.0, −3.1)	Cγ–Cβ	1.76 (1.71, 1.78)	−4.9 (−10.8, +0.9)
Cβ–Cδ	1.92 (1.90, 1.93)	−13.9 (−19.1, −5.1)	Cγ–Cδ	1.80 (1.78, 1.81)	−9.7 (−14.2, −6.6)
Cβ–Cε	1.94 (1.90, 1.98)	−6.0 (−14.6, +3.1)	Cγ–Cε	1.75 (1.74, 1.76)	−2.9 (−12.8, +0.4)
Cβ–Cγ	1.85 (1.80, 1.87)	−11.7 (−21.4, 0.0)	Cγ–Cγ	1.94 (1.90, 1.97)	+1.3 (−0.2, +5.0)
Cβ–Co	1.97 (1.95, 2.00)	−14.7 (−16.8, −12.1)	Cγ–Co	1.59 (1.55, 1.61)	+1.5 (−1.6, +6.7)
Cδ–Cα	1.95 (1.91, 1.97)	−6.2 (−11.4, −1.9)	Co–Cα	2.02 (2.00, 2.03)	+0.3 (−2.4, +5.6)
Cδ–Cβ	1.97 (1.95, 1.99)	+6.9 (+2.0, +13.5)	Co–Cβ	2.02 (2.00, 2.03)	+5.1 (1.0, +10.9)
Cδ–Cδ	1.89 (1.83, 1.90)	−1.0 (−7.4, +5.7)	Co–Cδ	2.03 (1.99, 2.06)	−3.0 (−6.8, +0.7)
Cδ–Cε	1.94 (1.90, 1.96)	−5.2 (−12.7, +0.4)	Co–Cε	2.03 (2.01, 2.08)	−6.7 (−13.4, +1.3)
Cδ–Cγ	1.88 (1.85, 1.92)	−3.5 (−7.8, +2.5)	Co–Cγ	2.00 (1.96, 2.03)	+10.1 (+4.5, +17.8)
Cδ–Co	1.96 (1.93, 2.02)	+6.9 (+1.4, +9.9)	Co–Co	2.02 (1.99, 2.04)	−1.2 (−4.2, +0.7)

A summary of the average inherent sensitivity enhancements and line width properties of all peaks for the ten NUS DARR experiment compared to a US DARR experiment collected in an equivalent total experiment time. In parentheses are the lowest and highest values within the ten experiments, respectively. The data were processed under identical conditions and result in an equivalent RMS noise level in the frequency domain within 0.8 % error. The NUS schedule was based on a 230 Hz exponential decay. On average, the inherent sensitivity enhancement for all peaks is 1.90× and the line width is enhanced by 1.5 %. Tables corresponding to the each of the ten NUS experiments can be found in the supporting information

have performed an assessment of the effect of point removal from a uniformly sampled dataset. Using this approach, a NUS schedule was used (post acquisition) to sub-sample a uniformly sampled dataset. NUS schedules corresponding to 90, 80, 70, 60, 50, 40, 30, 25, 20, 10, and 5 % coverage were tested. In addition to the analysis of these sub-sampled data, we have collected two more experimental datasets, one with 50 % and another with 25 % sampling and with the number of scans in both cases equal to that in the uniformly sampled dataset. These datasets were collected for comparison to the sub-sampled US data since the number of scans cannot be varied when applying the NUS schedule post-acquisition.

For sub-sampled datasets, we have examined the linearity and the sensitivity enhancements with respect to the US data as a function of the extent of sparseness in the sampling. In these datasets, we expect the noise to scale as the square root of the number of sampled points (Ernst 1966). Indeed, as shown in Table 4, this was the case: for the eleven sub-sampled datasets examined, to within a maximum error of 3.4 %. The normalized enhancements calculated from these data varied between 1.05 for 90 % and 1.75 for 20 % coverage sampling schedules, as summarized in Table 4. Important to note is the fact that when 10 % or fewer points are retained in the sampling schedule, the enhancements dropped to 1.66 (10 %) and 1.53 (5 %), lower than those found for 20 % sub-sampled data. This is due to the fact that when the schedules get this sparse, points need to be removed from the beginning of the FID, where the signal is the strongest.

Figure S6 of the Supporting Information shows correlation plots for the relative peak intensities of the sub-sampled DARR experiments on U-^{13}C,^{15}N-His where the number of retained points ranges from 90 to 5 % relative to the original number of points in the US spectra. It is obvious from the plots that when 40–90 % of the original points are retained, the linearity is also retained in the resulting sub-sampled datasets. Figure S7 displays the correlation between peak intensity in US/MINT versus NUS/MINT for 50 % sub-sampled and 50 % NUS DARR data. The results reveal that the errors in slope are very small, 2.1 % for the NUS data (red) and 0.1 % for the sub-

Table 4 Inherent sensitivity enhancement for sub-sampled NUS DARR spectra of L-histidine

% sampling	Experimental noise (% error)	Theoretical noise (scaled as $\sqrt{}$time)	Points in indirect dimension	Average normalized signal-to-noise ratio
100	13.32	–	320	1.00
90	12.63 (0.1)	12.64	288	1.05
80	11.88 (0.3)	11.92	256	1.10
70	11.22 (0.7)	11.15	224	1.11
60	10.46 (1.4)	10.32	192	1.16
50	9.52 (1.1)	9.42	160	1.32
40	8.48 (0.6)	8.43	128	1.36
30	7.27 (0.4)	7.30	96	1.52
25	6.70 (0.6)	6.66	80	1.63
20	6.03 (1.1)	5.96	64	1.75
10	4.36 (3.4)	4.21	32	1.66
5	2.96 (0.6)	2.98	16	1.53

Summary of the average signal-to-noise ratio for sub-sampled NUS DARR spectra of L-histidine compared to a uniformly sampled datasets. The experimental noise under these conditions scales as the square root of the total number of points or total experiment time since the number of scans remains constant. The signal-to-noise ratio of the uniformly sampled dataset was normalized to be 1.00. An increase in the sensitivity was observed as points are removed until the number of retained points is 20 %. For 10 and 5 % sampling the signal-to-noise ratio was found to decrease due to the removal of points from the beginning of the FID

sampled data (black). The errors in the y-intercept are 1.4 and 1.7 % for the 50 % NUS data (red) and 50 % sub-sampled data (black), respectively. The corresponding R^2 values are 0.987 and 0.990. As illustrated in Figure S6, when the sampling coverage in the sub-sampled data is 20–30 % with respect to the US data, there appears to be a slight degradation in spectral linearity. A drastic deviation from linearity is observed when the number of retained points in the sub-sampled NUS data is 10 % or below. Comparison of the 25 % NUS and the corresponding sub-sampled data reveals that the peak intensities are generally in good agreement. The errors in slope are 7.2 and 7.5 % for the NUS and sub-sampled data, respectively. The corresponding errors in the y-intercept are 0.8 and 5.6 %. The corresponding R^2 values are 0.928 and 0.990.

The above result is a manifestation of two independent considerations: (1) the fraction of points that is retained with respect to the original number of points, and (2) the total number of remaining points with respect to the number of signals in the spectrum. When the NUS schedules are dense and have large uniform tracts the desired distribution is approached closely. When the NUS schedules are so dense that they still have large uniform tracts, then the desired distribution is approached closely as the schedules become sparser. However, once the uniform tracts disappear, a new regime of extreme sparseness is reached such that any further samples are removed prior to 1.26 T_2 (as there are none left after 1.26 T_2 except for the final sample) then indeed the schedule is not achieving the desired distribution and clearly the sensitivity will suffer. The degradation in linearity observed as more points are removed from the sampling grid is most likely due to the fact that point removal results in decreasing the "peak-to-sidelobe ratio" (PSR, defined as the ratio of the magnitude of the central, zero-frequency, component of the point spread function (PSF) to the magnitude of the largest non-zero-frequency peak in the PSF) thereby introducing frequency-dependent amplitude errors (Schuyler et al. 2013).

These results, together with the findings reported by us previously (Paramasivam et al. 2012; Sun et al. 2012), indicate that in homonuclear ^{13}C–^{13}C MAS correlation experiments, conservative sampling where 50 % of the points are retained (for spectral widths of 200 ppm and indirect-dimension evolution times of 10–20 ms) presents a reliable approach for collecting NUS data when a strict linear response is needed. Under these conditions, the spectral features (signal intensities, peak widths, enhancements) are reproducible, and large inherent time-domain sensitivity enhancements (twofold on average) are attained in each indirect dimension. On the other hand, even though more aggressive under-sampling (5–25 % NUS schedules) could give rise to possible additional enhancements or time savings, the reproducibility and reliability of the spectral linearity is noticeably degraded. It is important to establish the principles for the design of the most aggressive sampling schedules that reliably recapitulate the salient spectral features, for an arbitrary set of experimental conditions in a given sample; this study will be performed in the future.

Applications to proteins: 1–73-(U-^{13}C,^{15}N)/74–108-(U-^{15}N) thioredoxin reassembly

To examine the benefits of NUS in homonuclear spectra of proteins, we turned our attention to 1–73-(U-^{13}C,^{15}N)/74–108-(U-^{15}N) thioredoxin reassembly. This protein reassembly has been extensively studied in our laboratory and serves as an excellent model system for testing NUS methods. Thioredoxin reassembly represents a typical protein sample with multiple cross peaks of varying line widths in the DARR spectra and high dynamic range (ca. 32×).

Figure 6a, b displays 2D US and NUS DARR spectra of thioredoxin reassembly acquired with equivalent experiment time. It is clear from the figure that significant sensitivity enhancement is attained in the NUS/MINT

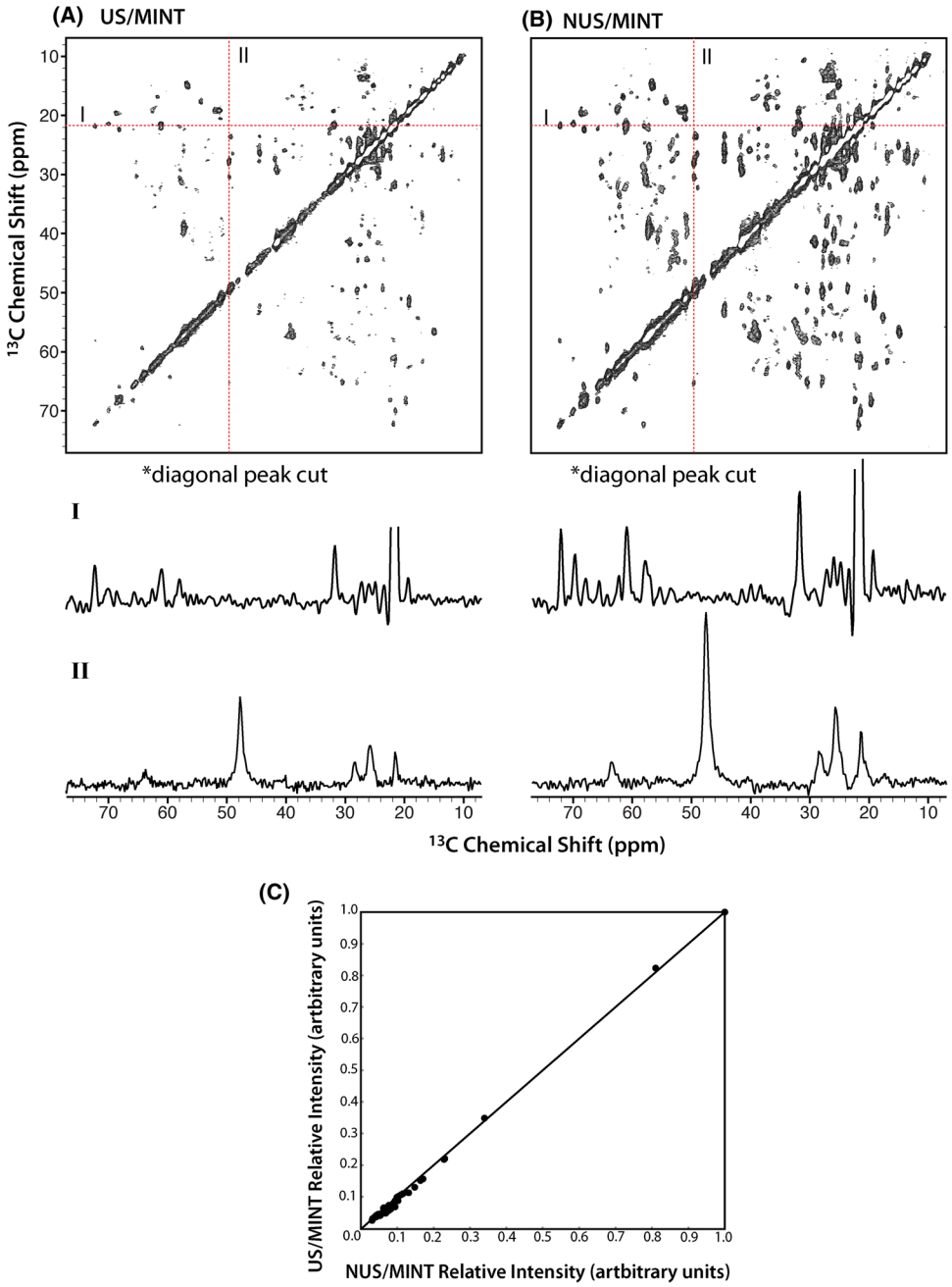

Fig. 6 **a** 2D DARR spectrum of 1–73-(U-^{13}C,^{15}N)/74–108-(U-^{15}N) thioredoxin reassembly collected with uniform sampling. **b** 2D DARR spectrum of 1–73-(U-^{13}C,^{15}N)/74–108-(U-^{15}N) thioredoxin reassembly collected with 50 % NUS. The spectra were acquired in an equivalent experiment time as (1,000 × 512) and (1,000 × 256) complex matrices with 16 and 32 scans per t_1 increment for US and NUS, respectively. The RMS noise levels are equivalent in the two datasets as measured using a signal-free region of the frequency domain spectra containing 52,224 samples. The first contour is displayed at 5× noise rmsd, and the level multiplier is 1.2. One-dimensional traces through the direct (*I*) and indirect (*II*) dimensions clearly illustrate the higher peak intensity in the NUS dataset. **c** Plot of relative NUS versus US cross-peak intensities for 2D DARR spectra of 1–73-(U-^{13}C,^{15}N)/74–108-(U-^{15}N) thioredoxin reassembly. The agreement between NUS and US relative peak intensities is excellent with the slope of 1.016 (1.6 % error), the y-intercept of −0.01 (1.0 % error), and the R^2 value of 0.998. Arbitrary units used for normalization

spectrum. In Fig. 6c, the relative intensities of the NUS spectrum are plotted vs. those in the US dataset. It is clear that the linearity is excellent under these conditions with the slope being equal to 1.02 (2 % error) and the y-intercept of −0.01 (1.0 % error). The R^2 value for the data is 0.998.

The intensity enhancement for the NUS experiment is 1.85 fold on average with values for individual peak enhancements ranging between 1.50 and 2.14 fold. There is no correlation between the degree of intensity enhancement and the absolute intensity of the individual peaks, as illustrated in Figure S2 of the Supporting Information. These results are in line with our observations for the model compounds.

The peaks in the NUS spectrum are on average 9.29 % broader with respect to the US dataset with values ranging from −11.1 Hz to 40.7 Hz. These results are similar to our prior findings for the heteronuclear datasets of the same sample. In the future, we will employ the line width deconvolution algorithm (Hoch and Stern 1996) to narrow line widths in this and similar protein datasets. Figure S3 (E) in the Supporting Information displays a scatter plot of absolute peak intensity versus line width difference (NUS–US) for this pair of spectra. There is no apparent trend between the two parameters. Comparisons of both sensitivity and line width between the NUS and US datasets are summarized in Table 5.

In summary, the results obtained for 1–73-(U-^{13}C,^{15}N)/74–108-(U-^{15}N) thioredoxin reassembly are encouraging. Under our experimental conditions, we have demonstrated that it is possible to reach significant (1.85×) inherent sensitivity gains in an experiment time equivalent to that in a conventionally uniformly sampled dataset. In addition, the linearity of the MINT transformation ensures that we obtain reliable results across the entire dynamic range. The increase in line width for the NUS dataset of 9.29 % on average, while non-negligible, is not severe enough to compromise the overall quality of the dataset. Line width deconvolution is expected to compensate for this moderate line broadening, based on our previous studies (Paramasivam et al. 2012). For

Table 5 Inherent sensitivity enhancement and line widths in NUS DARR spectra of 1–73-(U-^{13}C,^{15}N)/74–108-(U-^{15}N) thioredoxin reassembly

Correlation	NUS/MINT sensitivity enhancement	Line widths	Correlation	NUS/MINT sensitivity enhancement	Line widths
I5	1.60	3	P34	2.00	11.4
I5	1.89	11.7	A39	1.90	8.6
T6	1.61	−6.1	A39	1.97	6.3
T6	2.06	7.3	I45	1.72	14
T8	2.01	4	I45	1.77	6.3
T8	1.82	10.8	A46	2.13	2.6
S11	1.82	0.8	A46	1.89	3.3
S11	2.14	−6	A46	1.84	34.6
S11	1.75	26	A46	1.98	8.7
S11	1.99	3.1	T54	1.90	−5.4
T14	1.79	33.9	T54	2.06	8.6
T14	2.03	6.4	T54	1.55	−4.5
T14	1.92	20.3	T54	1.76	12.6
T14	1.80	2.4	A56	1.97	1.8
T14	1.55	3	A56	1.78	−1.2
T14	2.00	18.3	I60	1.78	12.7
V16	2.14	27.6	I60	2.08	−8.1
V16	1.50	3.1	I60	2.11	−11.1
V16	1.93	0.2	I60	1.51	40.7
V16	1.63	25.1	T66	1.83	34.6
I23	2.06	7.1	T66	1.56	−1.4
I23	1.86	23.6	P68	1.67	10.6
A29	1.87	8.3	P68	1.71	12.4
A29	1.88	9.1	P68	1.77	11.5
P34	1.69	28.2	P68	1.99	3.6
P34	1.77	33.7	P68	1.80	−10.5
P34	1.86	0.8	P68	1.85	1.1

A summary of the inherent sensitivity enhancements and line widths of the NUS DARR spectra of 1–73-(U-^{13}C,^{15}N)/74–108-(U-^{15}N) thioredoxin reassembly with respect to a US DARR spectrum collected with the same total experiment time. The data were processed under identical conditions; the RMS noise level is equivalent within 0.5 % as measured in the frequency domain. The NUS schedule is matched to a 100 Hz exponential decay

these reasons, we expect NUS to be useful for the studies of other proteins and protein assemblies.

Conclusions

This work establishes conservative recommendations for the use of nonuniform sampling to collect high-fidelity homonuclear ^{13}C–^{13}C MAS NMR datasets of high dynamic range, an important class of experiments that have not previously been considered for NUS/MINT methods. NUS schedules need to be carefully constructed so that the exponential weighting profiles follow the average decay rate of the signals in the sample. With conservative (50 %) removal of data points, high-quality datasets are produced with remarkably high linearity, large inherent sensitivity enhancements that agree with theoretical predictions, and retained line widths. More aggressive under-sampling may be an option where time savings are desirable but can give rise to increased discrepancies in spectral linearity with respect to the US datasets. While we found that these discrepancies may still be tolerable when sampling in the range of 20–40 %, caution must be exercised in quantitative interpretation of the results. In the future, we will systematically examine the dependence of sensitivity enhancements on the schedule sparseness and peak frequency. Overall, the work reported here in conjunction with our recent report demonstrates that NUS/MINT approach is applicable and highly beneficial to many homo- and heteronuclear multidimensional MAS NMR experiments, and we anticipate its growing use in a variety of interesting and important biological systems particularly those where sensitivity is a challenge.

Acknowledgments This work was supported by the National Institutes of Health (NIH Grants R01GM085306, P50GM082251, and P30GM103519 from NIGMS, and P30RR031160 from NCRR), and by Agilent University Collaborative Research award. We acknowledge the support of the National Science Foundation (NSF Grant CHE0959496) for the acquisition of the 850 MHz NMR spectrometer at the University of Delaware. The 21.1 T spectra were acquired at the Environmental Molecular Sciences Laboratory, a national scientific user facility sponsored by the United States Department of Energy's Office of Biological and Environmental Research and located at the Pacific Northwest National Laboratory in Richland, WA. The kind assistance of Andrew Lipton, Sarah Burton, Jesse Sears, Michael Froehlke, and Joseph Ford during our visit to EMSL is gratefully acknowledged.

References

Atreya HS, Szyperski T (2005) Rapid NMR data collection. Methods Enzymol 394:78–108

Balsgart NM, Vosegaard T (2012) Fast forward maximum entropy reconstruction of sparsely sampled data. J Magn Reson 223:164–169

Coggins BE, Venters RA, Zhou P (2010) Radial sampling for fast NMR: concepts and practices over three decades. Prog Nucl Magn Reson Spectrosc 57:381–419

Daniell GJ, Hore PJ (1989) Maximum entropy and NMR, a new approach. J Magn Reson 84:515–536

Davies SJ, Bauer C, Hore PJ, Freeman R (1988) Resolution enhancement by nonlinear data processing. "HOGWASH" and the maximum entropy method. J Magn Reson 76:476–493

Dereppe JM, Jakus N (1988) Maximum entropy spectral analysis of NMR signals of solids. J Magn Reson 79:307–317

Donoho DL, Johnstone IM, Stern AS, Hoch JC (1990) Does the maximum entropy method improve sensitivity? Proc Natl Acad Sci USA 87:5066–5068

Eghbalnia HR, Bahrami A, Tonelli M, Hallenga K, Markley JL (2005) High-resolution iterative frequency identification for NMR as a general strategy for multidimensional data collection. J Am Chem Soc 127:12528–12536

Ernst RR (1966) Sensitivity enhancement in magnetic resonance. Adv Magn Reson 2:1–135

Franks WT, Atreya HS, Szyperski T, Rienstra CM (2010) GFT projection NMR spectroscopy for proteins in the solid state. J Biomol NMR 48:213–223

Goddard TD, Kneller DG (2004) SPARKY 3. University of California, San Francisco

Hiller S, Fiorito F, Wuthrich K, Wider G (2005) Automated projection spectroscopy (APSY). Proc Natl Acad Sci USA 102:10876–10881

Hoch JC (1985) Maximum entropy signal processing of two-dimensional NMR data. J Magn Reson 64:436–440

Hoch JC, Stern AS (1996) NMR data processing. Wiley-Liss, New York

Hoch JC, Stern AS, Donoho DL, Johstone IM (1990) Maximum entropy reconstruction of complex (phase-sensitive) spectra. J Magn Reson 86:236–246

Hoch JC, Maciejewski M, Mobli M, Schuyler A, Stern AS (2012) Nonuniform sampling in multidimensional NMR. In: Harris RK, Wasylishen RE (eds) Encyclopedia of nuclear magnetic resonance, vol 6. Wiley, Chichester, pp 2999–3013

Holland DJ, Bostock MJ, Gladden LF, Nielispach D (2011) Fast multidimensional NMR spectroscopy using compressed sensing. Angew Chem 50:6548–6551

Hore PJ (1985) NMR data processing using the maximum entropy method. J Magn Reson 62:561–567

Hyberts SG, Heffron GJ, Tarragona NG, Solanky K, Edmonds KA, Luithardt H, Fejzo J, Chorev M, Aktas H, Colson K, Falchuk KH, Halperin JA, Wagner G (2007) Ultrahigh-resolution H-1–C-13 HSQC spectra of metabolite mixtures using nonlinear sampling and forward maximum entropy reconstruction. J Am Chem Soc 129:5108–5116

Hyberts SG, Frueh DP, Arthanari H, Wagner G (2009) FM reconstruction of non-uniformly sampled protein NMR data at higher dimensions and optimization by distillation. J Biomol NMR 45:283–294

Hyberts SG, Milbradt AG, Wagner AB, Arthanari H, Wagner G (2012) Application of iterative soft thresholding for fast reconstruction of NMR data non-uniformly sampled with multidimensional poisson gap scheduling. J Biomol NMR 52:315–327

Jaravine VA, Ibraghimov I, Orekov VY (2006) Removal of a time barrier for high-resolution multidimensional NMR spectroscopy. Nat Met 3:605–607

Jeong GW, Borer PN, Wang SS, Levy GC (1993) Maximum-likelihood-constrained deconvolution of two-dimensional NMR spectra. Accuracy of spectral quantification. J Magn Reson 103:123–134

Jiang B, Jiang XW, Xiao N, Zhang X, Jiang L, Mao XA, Liu ML (2010) Gridding and fast fourier transformation on non-uniformly sparse sampled multidimensional NMR data. J Magn Reson 204:165–168

Jones DH, Opella SJ (2006) Application of maximum entropy reconstruction to PISEMA spectra. J Magn Reson 179:105–113

Kazimierczuk K, Stanek J, Zawadzka-Kazimierczuk A, Kozminski W (2010) Random sampling in multidimensional NMR spectroscopy. Prog Nucl Magn Reson Spectrosc 57:420–434

Kim S, Szyperski T (2003) GFT NMR, a new approach to rapidly obtain precise high-dimensional NMR spectral information. J Am Chem Soc 125:1385–1393

Kupce E, Freeman R (2003) Projection-reconstruction of three-dimensional NMR spectra. J Am Chem Soc 125:13958–13959

Laue ED, Skilling J, Staunton J, Sibisi S, Brereton RG (1985) Maximum entropy method in nuclear magnetic resonance spectroscopy. J Magn Reson 62:437–452

Lin EC, Opella SJ (2013) Sampling scheme and compressed sensing applied to solid-state NMR spectroscopy. J Magn Reson 237C:40–48

Maciejewski MW, Stern AS, King GF, Hoch JC, Webb GA (2006) Nonuniform sampling in biomolecular NMR modern magnetic resonance. Springer, Netherlands

Malmodin D, Billeter M (2006) Robust and versatile interpretation of spectra with coupled evolution periods using multi-way decomposition. Magn Reson Chem 44:S185–S195

Mandelshtam VA, Taylor HS, Shaka AJ (1998) Application of the filter diagonalization method to one- and two-dimensional NMR spectra. J Magn Reson 133:304–312

Mansfield P (1984) Spatial-mapping of the chemical-shift in NMR. Magn Reson Med 1:370–386

Marulanda D, Tasayco ML, McDermott A, Cataldi M, Arriaran V, Polenova T (2004) Magic angle spinning solid-state NMR spectroscopy for structural studies of protein interfaces. Resonance assignments of differentially enriched *Escherichia coli* thioredoxin reassembled by fragment complementation. J Am Chem Soc 126:16608–16620

Marulanda D, Tasayco ML, Cataldi M, Arriaran V, Polenova T (2005) Resonance assignments and secondary structure analysis of *E. coli* thioredoxin by magic angle spinning solid-state NMR spectroscopy. J Phys Chem B 109:18135–18145

Matsuki Y, Eddy MT, Herzfeld J (2009) Spectroscopy by integration of frequency and time domain information for fast acquisition of high-resolution dark spectra. J Am Chem Soc 131:4648–4656

Matsuki Y, Eddy MT, Griffin RG, Herzfeld J (2010) Rapid three-dimensional MAS NMR spectroscopy at critical sensitivity. Angew Chem Int Ed 49:9215–9218

Paramasivam S, Suiter CL, Hou G, Sun S, Palmer M, Hoch JC, Rovnyak D, Polenova T (2012) Enhanced sensitivity by nonuniform sampling enables multidimensional MAS NMR spectroscopy of protein assemblies. J Phys Chem B 116:7416–7427

Rovnyak D, Filip C, Itin B, Stern AS, Wagner G, Griffin RG, Hoch JC (2003) Multiple-quantum magic-angle spinning spectroscopy using nonlinear sampling. J Magn Reson 161:43–55

Rovnyak D, Frueh DP, Sastry M, Sun ZJ, Stern AS, Hoch JC, Wagner G (2004) Accelerated acquisition of high resolution triple-resonance spectra using non-uniform sampling and maximum entropy reconstruction. J Magn Reson 170:15–21

Rovnyak D, Sarcone M, Jiang Z (2011) Sensitivity enhancement for maximally resolved two-dimensional NMR by nonuniform sampling. Magn Reson Chem 49:483–491

Schmieder P, Stern AS, Wagner G, Hoch JC (1993) Application of nonlinear sampling schemes to COSY-type spectra. J Biomol NMR 3:569–576

Schuyler AD, Maciejewski MW, Stern AS, Hoch JC (2013) Formalism for hypercomplex multidimensional NMR employing partial-component subsampling. J Magn Reson 227:20–24

Shrot Y, Frydman L (2011) Compressed sensing and the reconstruction of ultrafast 2D NMR data: principles and biomolecular applications. J Magn Reson 209:352–358

Sibisi S, Skilling J, Brereton RG, Laue ED, Staunton J (1984) Maximum entropy signal processing in practical NMR spectroscopy. Nature 311:446–447

Sun S, Yan S, Guo C, Li M, Hoch JC, Williams JC, Polenova T (2012) A time-saving strategy for MAS NMR spectroscopy by combining nonuniform sampling and paramagnetic relaxation assisted condensed data collection. J Phys Chem B 116:13585–13596

Takegoshi K, Nakamura S, Terao T (2001) 13C–1H dipolar-assisted rotational resonance in magic-angle spinning NMR. Chem Phys Lett 344:631–637

Yang J, Paramasivam S, Marulanda D, Cataldi M, Tasayco ML, Polenova T (2007) Magic angle spinning NMR spectroscopy of thioredoxin reassemblies. Magn Reson Chem 45:S73–S83

Yang J, Tasayco ML, Polenova T (2008) Magic angle spinning NMR experiments for structural studies of differentially enriched protein interfaces and protein assemblies. J Am Chem Soc 130:5798–5807

Yang J, Tasayco ML, Polenova T (2009) Dynamics of reassembled thioredoxin studied by magic angle spinning NMR: snapshots from different time scales. J Am Chem Soc 131:13690–13702

Zhang F, Bruschweiler R (2004) Indirect covariance NMR spectroscopy. J Am Chem Soc 126:13180–13181